

Using the spectral scaling exponent for validation of quantitative precipitation forecasts

T.-Y. Koh

School of Physical and Mathematical Sciences, Nanyang Technological University, Singapore
Earth Observatory of Singapore, Nanyang Technological University, Singapore
Temasek Laboratories, Nanyang Technological University, Singapore

B. C. Bhatt

Temasek Laboratories, Nanyang Technological University, Singapore

K. K. W. Cheung

Department of Environment and Geography, Macquarie University, Australia

C. K. Teo

Temasek Laboratories, Nanyang Technological University, Singapore

Y. H. Lee

School of Electrical and Electronic Engineering, Nanyang Technological University, Singapore

Matthias Roth

Department of Geography, National University of Singapore, Singapore

Purnawirman

Temasek Laboratories, Nanyang Technological University, Singapore

Corresponding address:

B. C. Bhatt

9th storey Border X Block, Research Techno Plaza

Temasek Laboratories, Nanyang Technological University

Singapore 637553

Abstract

This study evaluates the spectral scaling of a heavy rainfall event and assesses the performance of Coupled Ocean/Atmosphere Mesoscale Prediction System (COAMPS) model in terms of the multiscale variability of rainfall in the temporal spectral domain. The event occurred over southern Malay Peninsula on 18 December 2006 and was simulated at high resolutions. 10, 5 and 1-minute aggregate rainfall data from rain gauge stations in Singapore and simulated rainfall sampled at different evaluation points on 0.9, 0.3 and 0.1 km grids were utilized. The simulated and observed rain rates were compared via Fourier and wavelet analyses. A scaling regime was noted in the observed rainfall spectra in the timescales between 60 min and 2 min. The scaling exponent obtained from the observed spectra has a value of about 2, which may be indicative of the physics of turbulence and raindrop coalescence and might suggest the predominance of a characteristic raindrop size. At 0.9 km resolution, the model rainfall spectra showed similar scaling to the observed down to about 10 min, below which a fall-off in variance was noted as compared to observations. Higher spatial resolution of up to 0.1 km was crucial to improve the ability of the model to resolve the shorter timescale variability. We suggest that the evaluation of dynamical models in the spectral domain is a crucial step in the validation of quantitative precipitation forecasts and assessing the minimal grid resolution necessary to capture rainfall variability for certain short timescales may be important for hydrological predictions.

1. Introduction

The characterization of the multiscale properties of rainfall fields is an important research area in hydrometeorology which seeks to understand rain patterns as a manifestation of the fractal geometry of nature (Mandelbrot 1982) and the underlying chaos of the atmosphere (Lorenz 1963). The scaling of the power density in the temporal spectra of rain may be related with the fractal dimension and the statistical properties of the rainfall time series itself (Abarbanel 1997), which are in turn reflections of the turbulent dynamics during a rainstorm. Thus, the power-law scaling exponent of rainfall spectra can, in principle, be used as verification diagnostic for model storm simulations.

Current diagnostics on the quantitative precipitation forecast (QPF) skill for numerical weather prediction (NWP) models are carried out in the spatio-temporal domain (\mathbf{x}, t): e.g. Junker et al. (1992); White et al. (1999); McBride and Ebert (2000) ; Cherubini et al. (2002) ; Ebert et al. (2003) and Marzban and Sandgathe (2009). Common QPF diagnostics used include: Frequency Bias index (FBI); Probability of Detection (POD); False Alarm Rate (FAR); Threat Score (TS) or its improved variant, Equitable Threat Score (ETS); True Skill Statistic (TSS), also known as Hanssen-Kuipers (HK) discriminant; variograms and so on. A review of these statistics can be found in Chapter 7 of Wilks (2006). Scale-decomposition verification techniques, e.g. Casati et al. (2004) and Csima and Ghelli (2008), and Root-Mean-Square Error (RMSE) measures, e.g. White et al. (1999) and Mullen and Buizza (2001), have been used. But RMSE is heavily influenced by the inherent variability of the diagnosed variable itself and should be supplanted by the bias-adjusted and normalized Alpha Index, as explained in Koh and Ng (2009). Regardless of the diagnostic used, individual NWP models and even ensemble prediction systems almost always perform badly in QPF, even when skill is demonstrated for other variables like wind and temperature. Or perhaps, might it not be possible that we are lacking in the skill of diagnosing QPF performance?

In this paper, we put forth an idea to assess QPF performance in the spectral domain. Direction or phase errors in the wavenumber (\mathbf{k}) space and phase errors in frequency (ω) space correspond to discrepancies in rain pattern, location and time of occurrence in (\mathbf{x}, t) domain, i.e. the

very measures which are hard to forecast at storm scales but are ironically assessed by conventional QPF diagnostics. In fact, the sensitivity to initial conditions so characteristic of chaotic systems may suggest that accurate information on these aspects of mesoscale storms might never be truly feasible much ahead of time. We suggest as a step in NWP development at cloud-resolving scales to verify the power density of rainfall spectra, for the distribution of variance across spatial and temporal scales is a more direct indicator of storm dynamics. From the point of view of *dynamical* modelling, getting the scaling exponent right in the spectra is a necessary step to make good predictions. An ensemble approach is inherently adopted here as spectra from a set of observations (at fixed time or space) are collectively compared to those from the model, because the statistical theories of spectral scaling fundamentally require an ensemble-average concept.

Many investigators characterized the multiscaling behavior of rainfall over a range of spatio-temporal scales (Gupta and Waymire 1990; Tessier et al. 1993; Kumar and Foufoula-Georgiou 1993; Venugopal et al. 1999; Harris et al. 2001; Nykanen and Harris 2003; Lovejoy et al. 2008; Beecham and Chowdhury 2010). For this preliminary work, we focus on temporal spectral analysis at fixed locations where we have high-resolution rain gauge data, relegating spatial spectral analysis as our next endeavor.

The first question on the scaling of rainfall power spectra concerns the analogue to the “inertial range” of classical three-dimensional turbulence. Within this range of frequency f , the spectral power density P of rain rate varies as follows:

$$P(f) \propto f^{-\beta} \quad (1)$$

Rainfall data from a variety of observational platforms have been used in past studies, e.g. optical rain gauge (Georgakakos et al. 1994), sonic rain gauge (Fabry 1996), dropper rain gauge (Menabde 1997), radar (Hsu et al. 2006) and lidar (Mandapaka et al. 2009). The studies were carried out in different geographic regions and seasons, e.g. warm-season precipitation over North America (Hsu et al. 2006) or Germany (Fraedrich and Larnder 1993) and winter rainfall at Norfolk island, New Zealand (Menabde 1997). They include both stratiform and convective rain (Nikolopoulos et al. 2008) and involve different meteorological systems, e.g. the rain-band of a subtropical cyclone passing over North Island, New Zealand (Menabde 1997). Allowing for the limitations arising from the resolution and length of the time series, these studies reveal that power-law scaling for rainfall occurs within the

period range from the lower bound of a few seconds (Fabry 1996; Mandapaka et al. 2009), tens of seconds (Georgakakos et al. 1994; Nikolopoulos et al. 2008), or several minutes (Menabde 1997) to the upper bound of about one hour (Fabry 1996; Nikolopoulos et al. 2008), part of a day (12 hours for Hsu et al. 2006; 17 hours for Menabde 1997) or a few days (Fraedrich and Larnder 1993).

The next question on the value of the scaling exponent β arises naturally and there is less agreement among different authors in the literature on the answer. For kinetic energy and passive scalars, the respective theoretical analyses of Kolmogorov (Kolmogorov 1941, 1962) and Corrsin-Obukhov (Corrsin 1951; Obukhov 1949) imply that $\beta = 5/3$ when the turbulence is three-dimensional, homogeneous and isotropic. For rain rate, which is the product of raindrop number density, volume and terminal fall velocity, integrated over all raindrop sizes, a theoretical prediction is harder to achieve and has not been found in the literature.

As for empirical estimates of the scaling exponent, Olsson et al. (1993) analyzed 1-minute resolution rainfall data collected over two years 1979-1980 at 12 locations in the city of Lund, Sweden. They reported that the power spectrum is scale-invariant with $\beta = 5/3$ up to 50 min. Fraedrich and Larnder (1993) analyzed rainfall time series of 5-minute resolution in Germany for May to September 1975-87. They showed $\beta = 1/2$ for periods shorter than 3 days. Harris et al. (1996) investigated the orographic influence on the multiscaling properties of the 15-second resolution rainfall time series collected by rain gauges during June 1993, May 1994, and November 1994 in Southern Alps, New Zealand and found that the scaling regime depended on the elevation of the rain gauge and β can range from 0.9 to 1.7. The scaling exponents β estimated elsewhere in the literature lie between 1.36 and 3.34 in Nikolopoulos et al. (2008), between 1.2 and 1.4 in Georgakakos et al. (1994) and around 1.4 in Fabry (1996). Given the diverse range of empirical values, the consensus understanding may be that the scaling exponent β depends on the rain-generating mechanism which varies with the regional climate as well as the local environment. However, the inability of most instruments to accurately distinguish between zero and light rain rates may also explain in part the wide divergence of estimates of β in the literature (Verrier et al. 2010).

Some other investigators examined the scaling of log-rain rate rather than that of rain rate itself. Crane (1990) analyzed the 30-second rain gauge time series of all storms in Germany for 1979 and demonstrated spectral slopes close to 3 and $5/3$ for periods up to 3 min and 30 min respectively. Veneziano et al. (1996) used the same dataset as in Georgakakos et al. (1994) and concluded that while rainfall conforms to a multiplicative model, i.e. it is the product of independent non-negative variations of different temporal scales, the type of self-similarity manifested is less strict than that characteristic of multifractal models. This is because spectral slopes of 1 for log-rain rates, proven for multifractal models in Appendix A1 of Veneziano et al. (1996), are not realized.

While most of the surveyed literature examined mid-latitude rainfall, there is some evidence that tropical rainfall may possess different characteristics. By comparing gauge rainfall time series of up to 6-hour resolution, Sivakumar (2000) showed differences for the box dimension of intense rain occurrence between Singapore ($1^{\circ}20'N$) and Leaf River basin ($31^{\circ}42'N$), Mississippi, USA. (Whether the low box dimension found in both cases is indicative of deterministic chaos, or rainfall is really a stochastic process, is much debated issue, e.g. Sivakumar et al. (1998), Schertzer et al. (2002). But this interesting question lies outside the scope of our work.) In the tropics where our work lies, due to the relative unavailability of high-resolution rain gauge data, knowledge of sub-hourly rainfall variability over land has been rather lacking. In recent years, high-frequency rain gauges and radars capable of 10-min resolution or less have been widely installed by national meteorological agencies in tropical Southeast Asia (Koh and Teo 2009). Therefore, the timing seems right to pose our first question: how does rainfall variance behave at sub-hourly timescales in tropical storms?

At the same time, the dynamical simulation of rainfall at high resolution is now easily achievable, as a result of the advancement in computational speed and increasing affordability of computational clusters. However, given the inherent sensitivity of weather to initial conditions, the paucity of high-resolution data used in analysis and assimilation, and the uncertainties in model representations of storm dynamics, cloud microphysics and sub-grid turbulence, one may genuinely ask: do NWP models demonstrate skill in QPF at cloud-resolving scales? This second question is most poignant in the tropics where mesoscale convection dominates the weather throughout the year.

A preliminary attempt is made herein to address the above two questions by (1) investigating the existence of temporal scaling behavior in sub-hourly rain gauge data in a tropical storm; and (2) comparing with the scaling within the QPF produced by a mesoscale model. The chosen case study is a heavy rainfall episode that occurred in Singapore and nearby southern Malay Peninsula during 17-20 December 2006, which resulted in severe flooding (Tangang et al. 2008). To reiterate, accurate prediction of the spatio-temporal location or pattern of the rain system is of less relevance here. The focus is on whether the multiscaling property of tropical rainfall is correctly reproduced in the cloud-resolving model.

In section 2, we describe the study area and rainfall data from observations and modelling. Section 3 provides the spectral analysis methods. Section 4 is devoted to the results. Finally, the main conclusions and discussions are in section 5.

2. Observed and Model Data

Singapore situated at the southern tip of the Malay Peninsula in Southeast Asia was selected as the study area (Fig. 1, lower panel). There are small mountainous land masses and bodies of water distributed over this region. The monsoon encroach the Malay Peninsula from the northeast direction at low levels from mid-November to mid-March, and reverses to southwesterly flow from mid-May to early October. While thunderstorms occur throughout the year (Lim and Samah 2004; Joseph et al. 2008), the average monthly rainfall is the highest in December during the northeast monsoon (Sivakumar 1998; Lim and Samah 2004). It was during this rainiest part of the year that the heavy rainfall event on 18 December 2006 was recorded.

2.1 Rainfall observations

Data were collected from 8 rain gauges of tipping-bucket type in Singapore (Fig. 1, lower panel). The rain gauges R1 to R8 were chosen for their fine-resolution temporal sampling. The continuously available rainfall time series for the R1 station at Nanyang Technological University

(NTU) was less than 17 hours long starting from 0800 LT at 1-minute intervals on 18 December 2006. An unbroken 24-hour rainfall record starting at 0800 LT on the same day at 5-minute intervals was obtained from the R2 station at National University of Singapore (NUS). Continuous rainfall data at 10-minute resolution for 24 hours were obtained from the other 6 stations over Singapore maintained by Meteorological Services Division (MSD), National Environment Agency, Singapore. The peak rainfall rates recorded by these rain gauges all exceed 10 mm per 10 min. Additionally, MSD provided radar reflectivity data from the Changi weather radar (103.989°E, 1.359°N) at approximately 1-minute resolution with only occasional data gaps for the duration of the event.

2.2 Model simulation

The model used in this study was the Coupled Ocean/Atmosphere Mesoscale Prediction System (COAMPS[®]) developed by Naval Research Laboratory at Monterey, CA, USA. The atmospheric model uses non-hydrostatic primitive equations and has parameterization schemes for radiation, multi-phase cloud microphysics, cumulus convection (at resolutions coarser than 10km), turbulence and surface-layer processes (Hodur 1997). For the simulation reported here, only the atmospheric analysis and forecast component of COAMPS was integrated, with one-way nesting over multiple domains. The initial and boundary conditions were provided by the Navy Operational Global Atmospheric Prediction System (NOGAPS).

The experimental set-up consisted of six nested domains at resolutions of 24.3 km, 8.1 km, 2.7 km, 0.9 km, 0.3 km, and 0.1 km (Fig. 1, upper panel). There were 75 model vertical levels with enhanced resolution of the boundary layer. A time step of 30 seconds was used on the outermost domain and the time step was reduced to one third from each outer to the next inner domain. The choice of smaller time step was important to simulate the highly convective weather, i.e. heavy rainfall case, over the tropical maritime continent. Two 12-h assimilation-forecast cycles were carried out to spin up the model before initialization at 0000 UTC (or 0800 LT) on 18 December 2006 for a continuous 24-h forecast. The data assimilation technique used by COAMPS (version 3.1.1) is the Multivariate Optimal Interpolation (Barker 1992) and conventional data like radiosonde and surface

station (excluding rain gauge) and satellite data like isobaric layer thickness and cloud-tracked wind have been assimilated. The model rainfall output was at 1-minute interval.

Being interested in the temporal variability of rainfall, the rainfall fields were sampled at the nearest grid points to the rain gauges and at selected evaluation points in all three inner nests of sub-kilometer resolution. The evaluation points for nest 4 are displayed in Fig. 2. They were chosen to sample the sea, land and coastal regions, and to lie in the rainy areas of the squall as seen from the animation of radar and model simulation images.

3. Methods of Spectral Analysis

The Discrete Fourier Transform (DFT) is an elementary spectral method used to transform a time series into a superposition of sinusoidal variations of discrete frequencies with information on the variance and phase at each frequency. Its implementation in this work follows that of Torrence and Compo (1998). The advantage of DFT is that it is relatively simple to comprehend and can be implemented efficiently using the Fast Fourier Transform algorithm (Press et al. 1992). The drawback is that the sinusoidal basis may not be the best suited to capture rainfall variability as the onset or intensification of rainfall tends to be abrupt. Fourier spectra can also be sensitive to the global trends across the finite time domain of the dataset.

Wavelet analysis is particularly useful in identifying spectral properties of time series containing shifts, breakdown points and discontinuities (Torrence and Compo 1998). The wavelet analysis decomposes a time series into basis functions localized in frequency and time and is capable of local descriptions of segments in the time domain of the dataset. Our implementation again follows that of Torrence and Compo (1998), using the Morlet wavelet as it is usual in rainfall analyses. But as verification in the time domain is not the objective of this work, we sum up the variance for wavelets of the same frequency to obtain an equivalent spectral power density at that frequency which can be compared with the Fourier spectrum. This wavelet spectrum has the advantage that it is much smoother than the Fourier spectrum and thus is useful for the next step.

To find the scaling exponent β as in equation (1), the spectral power density $P(f)$ from wavelet analysis was plotted against frequency f on a log-log scale and a straight line was fitted to the scaling range by the least-square method (Wilks 2006), i.e.

$$\log P(f) = \beta \log f + \text{constant} \quad (2)$$

The wavelet, not the Fourier spectrum, is selected for this fitting because it is the smoother between the two. Moreover, the wavelet spectrum was seen to capture the essential variation of Fourier spectral power density across frequencies.

All observed and modeled rainfall datasets were analyzed over 24 hours starting from 0800 LT on 18 December 2006. The only exception was for R1 station: the observed and modeled time series were only 16 hours long and started later from 0820 LT to ensure that rainfall is zero at the end time like for all other stations. Truncating rainfall series at non-zero values can distort the variance at high frequencies because DFT implicitly repeats the sampled time window ad infinitum and non-zero start and end values, unless matching, would introduce artificial discontinuities across the edges of the time window. In pre-processing the observed and model data for spectral analyses, the 1-min resolution series were temporally aggregated into 5-min series and the 5-min series were aggregated into 10-min series, so that multiple resolutions of the same rainfall data were obtained.

4. Results

4.1 Model performance in spatio-temporal domain

The model performance in spatio-temporal domain (\mathbf{x}, t) was briefly assessed first by comparing with rainfall observations from the radar and rain gauges. A sample comparison at 2230 LT on 18 December 2006 between the simulated rainfall from nest 4 at 0.9 km resolution and the radar reflectivity at 0.81° elevation angle interpolated onto 1-km grid is shown in Fig. 2. Radar observations showed the squall line to be moving from the northeast direction over southern Malay Peninsula, while the simulated rainfall arrived the earliest at point 4 and before arriving in order at points 5, 7, 11, 10, 3,

9, 2, 6, 8 and 1. Thus the simulated squall movement is in general agreement with the radar observations. Moreover, the simulated rainfall development was similar to the observed in terms of the overall structure, e.g. the three patches of precipitation (north, south and east) in nest 4 have corresponding counterparts in the radar reflections in Fig. 2b. However, specific differences between the size, pattern and location of the rainfall patches can still be discerned as expected for a forecast at such high resolution. These spatial disagreements are related to the temporal differences described next.

The rainfall time series from the rain gauges were compared with those at the nearest grid point in the model nest 4 in Fig. 3. Although the comparison cannot be made below the measurement precision of the rain gauge, it is obvious that episodes of rainfall intensification do not generally coincide between the model and observations. There are also differences in onset times of rainfall: about 2 hours for R8 station in eastern Singapore (Figs. 3a-b) and about 1/2 hour at R2 and R1 stations in western Singapore (Figs. 3c-d and Figs. 3e-f respectively). Such comparisons reveal inconsistent model performance in predicting the time of occurrence of rainfall. The time-mean rainfall rate is also generally lower in the model than what is observed.

The above comparisons in (\mathbf{x}, t) domain demonstrates very well the motivation for validating the model performance in the frequency f domain. The focus there is on the spectral power density of the time-varying components (i.e. not the zero-frequency or mean component), ignoring the information on phase in Fourier analysis or not distinguishing between components that differ only in the location index in wavelet analysis.

4.2 Spectral analysis of observed rainfall

Fourier and wavelet analysis were applied on the observed and simulated 10-min rainfall time series of 10-min resolution at stations R1 to R8. To illustrate, the panels on the left column of Fig. 4 show the Fourier and wavelet power spectra from the observed rainfall at R1, R4, R6 and R8 stations located at the four corners of Singapore. The wavelet spectra clearly reflect the same essential trend of spectral power across the frequencies as the Fourier spectra. Least-square fit to obtain the scaling

exponent β was applied to each observed wavelet spectra for periods between 60 and 20 min which is the shortest period. The spectra for periods longer than 60 min are too coarsely resolved to be representative of the scaling.

Figure 5 summarizes the values of β obtained from the wavelet spectra of available observations at all stations. The least-square fit was carried out consistently for periods from 60 min down to the shortest resolvable period. For the 10-min and 5-min datasets, a best-estimate value of β could be further obtained from the arithmetic mean of the estimates for all available stations, i.e. from 8 and 2 stations respectively. These two best estimates are fitted to different scaling ranges, [60, 20] and [60, 10] min, and have values $\beta_{10\text{min}} = 2.02 \pm 0.12$ and $\beta_{5\text{min}} = 1.67 \pm 0.09$ respectively. While the latter estimate agrees well with the classic 5/3 power law for passive scalars, the former is steeper than 5/3. The 1-min data at R1 station estimates $\beta_{1\text{min}} = 1.33 \pm 0.11$ which is gentler than 5/3. For station R1, there seems to be an increase in the variability of slope estimate for from 1-min through to 10-min rainfall accumulation. As this is only seen in one station, it is hard to ascertain its significance without more 1-min gauge datasets are obtained (but such high temporal resolution datasets are rare). As it is dubious whether results from one or two stations could be representative, the balance of the evidence in this work suggests that β may be closer to the value of 2 than 5/3.

4.3 Spectral analysis of model rainfall

The panels on the right column of Fig. 4 show the Fourier and wavelet spectra from the simulated rainfall in nest 4 at the grid points nearest to R1, R4, R6 and R8 stations. Both types of spectra are not too different from the scaling estimated from their corresponding rain gauge data (left column of Fig. 4) for periods shorter than 60 min. Fig. 6 shows a few examples of the results when the spectral analyses were extended to 10-min rainfall at the 11 model evaluation points in the nest 4. The spectra at a number of evaluation points exhibit scaling for periods shorter than 60 min that seem close to the best estimate $\beta_{10\text{min}}$ obtained from the 10-min rainfall observations. The agreement is further quantitatively tested in Fig. 7 by taking the arithmetic mean of the scaling exponents obtained for all evaluation points, $\beta_{N4,10\text{min}} = 1.83 \pm 0.19$, as the best estimate for nest 4's 10-min output, and comparing that with $\beta_{10\text{min}} = 2.02 \pm 0.12$ from the observations. $\beta_{N4,10\text{min}} - \beta_{10\text{min}} = -0.19 \pm 0.22$ is not significantly

different from zero and hence the hypothesis that the model captures the spectral scaling in the observations is acceptable.

The effect of horizontal resolution in the model is investigated next. The Fourier and wavelet spectra of 1-minute rainfall from the R1 station are shown in Fig. 8a, where the scaling exponent β was estimated for periods between 60 and 2 min. The spectra of the simulated rainfall at the model grid point nearest to the R1 station in the nest 4 at 0.9 km resolution is shown in Fig. 8b. A sharp fall-off in the modeled spectral power for periods shorter than 10 min is obvious in nest 4. Thus the model is fundamentally not capable of forecasts of rainfall variability within about 10 min at a horizontal resolution of 0.9 km, because the turbulent dynamics underlying rainfall variability is not correctly simulated. Similar analyses were extended for nests 5 and 6 at resolutions 0.3 and 0.1 km respectively in Figs. 8c-d. The scaling in spectral power between periods 60 and 2 min is improved with increasing horizontal resolution. But spectral power at periods shorter than 6 min is still weaker than in the observations. The scaling at other model evaluation points in nests 5 and 6 also show similar improvements over those in nest 4 (not shown).

In increasing horizontal resolution in the model, the time-steps have to be proportionately reduced to satisfy the Courant condition. So a question naturally arises: is the improvement in scaling seen above due to smaller time-step or smaller grid size being employed? Thus, the model simulation was repeated by employing only nests 1 to 4 in the model and reducing the time-steps for all four nests by a factor of 9 such that nest 4 now uses the same time-step (0.037 s) as nest 6 previously did. Figure 9 shows the power spectra at the model grid point nearest to the R1 station in nest 4 for this experiment. The same fall-off in spectral power appeared in the high frequencies as before. The same result is obtained at other model evaluation points (not shown). This proves that reducing time-step alone does not help to capture variance at short timescales or improve the spectral scaling. The implication is that high spatial resolution is essential to correctly simulate the turbulent dynamics of mesoscale rain systems.

5. Theoretical Discussion

While the main subject of this paper concerns the estimation of scaling exponent β in observed tropical rainfall and validating β in the cloud-resolving model outputs as a necessary step in QPF verification, it is relevant to discuss some of the theoretical implications of the work.

The scaling range of the gauge rainfall was noted to correspond to periods [60 min, 2 min] (Fig. 8a). The outer time limit of 60 min is likely to be an artifact associated with the finite length of the data time series of up to 1 day as longer-time variability is not well captured. In fact, Lovejoy et al. (2008) analyzed 75 days of tropical rainfall derived from TRMM satellite measurements and showed that the scaling range extends spatially to planetary scales $O(10^4 \text{ km})$ which, assuming an advection velocity of $O(10 \text{ m/s})$, may be interpreted as a timescale of $O(10 \text{ days})$. On the other hand, the inner time limit of 2 min is likely to be only an upper bound to the actual short timescale as it is imposed by the 1-min time resolution of the rain gauge.

Lovejoy and Schertzer (2008) reasoned that the number density of raindrops is affected by the coalescence process and the transfer time for number density variance flux between neighboring scales is effectively determined by the coalescence speed. Their derivation led to a theoretical scaling exponent of $\beta = 2$ for raindrop number density. As this value is very close to the empirical value of $\beta_{10\text{min}} = 2.02 \pm 0.12$ obtained earlier, one wonders if the problem of scaling exponent for rain rate could be simplified by considering that in tropical storms, the cumulative distribution function $N(V)$ of number density against raindrop volume V rises rapidly over a narrow range $[V_0 - \Delta V, V_0 + \Delta V]$ i.e. an overwhelming large fraction of the population of raindrops have characteristic volume around V_0 (Marzuki et al. 2010). Kozu et al. (2006) also noted similar behavior in raindrop size distributions from three different tropical sites namely: Gadanki (South India), Singapore and Kototabang (Indonesia). Tokay et al., (2002) made similar observations in southwest Amazon region of Brazil during the Tropical Rainfall Measuring Mission (TRMM) field campaign and at Darwin during the 1993-94 wet season. Thus, one may estimate that the terminal fall velocity w would also have a characteristic value w_0 associated with the raindrop size $V_0^{1/3}$ and so rain rate r can be approximated as

$$r = \int_{\text{all } V} V_w \frac{dN}{dV} dV \approx V_0 w_0 \left(\frac{dN}{dV} \right)_{V_0} \Delta V$$

$$\propto (\Delta N)_{V_0}$$

Hence, rain rate r is roughly proportional to number density ΔN of raindrops around the characteristic volume V_0 and so has a scaling exponent close to 2 for number density of raindrops. This theoretical argument is merely a plausible one suggested by the observed value of $\beta_{10\text{min}}$. More tropical rain gauge data and longer time series of higher time resolution are needed to confirm the value of β and the understanding implied.

6. Conclusions

Fourier and wavelet analyses were performed on high-resolution surface rainfall time series from rain gauges and the COAMPS model. The model rainfall fields were sampled at grid points nearest to the rain gauges as well as other evaluation points in the inner three nests at 0.9, 0.3 and 0.1 km horizontal resolution respectively. The simulated rainfall spectra were compared to the best-estimate scaling obtained by the least-square fit to the observed wavelet spectra. Our results show that: (1) Fourier and wavelet spectra show essentially the same scaling of spectral power density; (2) the scaling exponent $\beta_{10\text{min}} = 2.02 \pm 0.12$ estimated from 10-min rain gauge data is higher than the classical value of $5/3$ for passive scalar but close to the value of 2 for raindrop number density; (3) the 0.9-km grid in the model is able to reproduce the observed spectral scaling for periods between 60 and 20 min; (4) higher horizontal resolution, and not merely smaller time-steps, is essential to capture the spectral scaling for periods below 20 min; (5) nonetheless, the rainfall variance in COAMPS model is always weaker than the observed below a certain threshold timescale imposed by the finite grid size.

Compared to the scaling exponents estimated in the literature reviewed in Section 1 (Olsson et al. 1993; Fraedrich and Larnder 1993; Harris et al. 1996; Nikolopoulos et al. 2008; Georgakakos et al. 1994; and Fabry 1996), our estimate of β is reasonable and may be characteristic of tropical rain storms in southern Malay Peninsula, but more observations are needed to confirm this point. The importance of spatial resolution to simulate small-scale variability in models has been mentioned before by Harris

et al. (2001) and our experiments with increased horizontal and temporal resolution reinforced this point. While Crane (1990) and Fabry (1996) reported some noise spectrum at the highest frequencies, such noise is not apparent in our results. This may be because those authors had rainfall series of resolution on the order of seconds, which is much finer than what is available to us.

The steeper nature of our spectral scaling compared to the classic $5/3$ power-law is consistent with the fact that raindrops are not passive scalars. In fact, the proximity to the 2 power law for raindrop number density seems to suggest that raindrops in tropical storms may be predominantly of a characteristic size. As the scaling exponent β is indicative of the underlying turbulent dynamics of the particular type of weather system in a geographic region, it is important that dynamical models are validated for the rainfall variance in the spectral domain first, before they are evaluated for the accuracy in forecasting the occurrence, size and pattern of rain formation in the spatio-temporal domain. Such validation would also yield valuable information on the minimal grid resolution required if rainfall variability at a certain short timescale is to be well simulated such as for input into hydrological prediction systems, whereas conventional QPF verification methods would not be able to address this question.

The specific results presented here should be interpreted with a degree of caution, mainly because they are based on one case study. Analysis of more cases with different meteorological conditions is the next step in our work and the preliminary results seem promising.

Acknowledgements

The authors would like to thank Meteorological Services Division, National Environment Agency, Singapore for providing the rain gauge and radar reflectivity data. This work was supported by grants from Temasek Laboratories @ NTU.

References

- Abarbanel HD (1997) Analysis of Observed Chaotic Data. Springer, New York, pp284
- Barker E (1992) Design of the navy's multivariate optimum interpolation analysis system. *Wea. Forecasting* 7:220–231
- Beecham S, Chowdhury RK (2010) Temporal characteristics and variability of point rainfall: a statistical and wavelet analysis. *Int. J. Climatol.* 30:458-473
- Casati B, Ross G, Stephenson D (2004) A new intensity-scale approach for the verification of spatial precipitation forecasts. *Meteorol. Appl.* 11:141-154
- Cherubini TA, Ghelli A, Lalaurette F (2002) Verification of precipitation forecasts over the Alpine region using a high-density observing network. *Wea. Forecasting* 17: 238-249
- Corrsin S (1951) On the spectrum of isotropic temperature fluctuations in an isotropic turbulence. *J. Appl. Phys.* 22: 469–73
- Crane RK (1990) Space-time structure of rain rate fields. *J. Geophys. Res.* 95:2011-2020
- Csima G, Ghelli A (2008) On the use of intensity-scale verification technique to assess operational precipitation forecasts. *Meteorol. Appl.* 15:145-154
- Ebert EE, Damrath U, Wergen W, Baldwin M (2003) The WGNE assessment of short-term quantitative precipitation forecasts. *Bull. Amer. Meteor. Soc.* 84: 481-492
- Fabry F (1996) On the determination of scale ranges for precipitation fields. *J. Geophys. Res.* 101: 12819-12826

- Fraedrich K, Larnder C (1993) Scaling regimes of composite rainfall time series. *Tellus*, 45A: 289-298
- Georgakakos KP, Carsteanu AA, Sturdevant PL, Cramer JA (1994) Observation and analysis of Midwestern rain rates. *J. Appl. Meteorol.* 33:1433-1444
- Gupta VK, Waymire E (1990) Multiscaling properties of spatial rainfall and river distribution. *J. Geophys. Res.* 95:1999-2010
- Harris D, Menabde M, Seed A, Austin G (1996) Multifractal characterization of rain fields with a strong orographic influence. *J. Geophys. Res.* 101:26405-26414
- Harris D, Foufoula-Georgiou E, Droegemeier KK, Levit JJ (2001) Multiscale statistical properties of a high-resolution precipitation forecast. *J. Hydrometeor.* 2:406-418
- Hodur RM (1997) The Naval Research Laboratory's coupled Ocean/Atmosphere Mesoscale Prediction System (COAMPS). *Mon. Wea. Rev.* 125:1414-1430
- Hsu HM, Moncrieff MW, Tung WW, Changhai L (2006) Multiscale temporal variability of warm-season precipitation over North America: statistical analysis of radar measurements. *J. Atmos. Sci.* 63:2355-2368
- Joseph B, Bhatt BC, Koh TY, Chen S (2008) Sea breeze simulation over Malay Peninsula over an intermonsoon period. *J. Geophys. Res.* 113:D20122, doi:10.1029/2008JD010319
- Junker NW, Hoke JE, Sullivan BE, Brill KF, Hughes FJ (1992) Seasonal and geographic variations in quantitative precipitation prediction by NMC's Nested-Grid Model and medium-range forecast model. *Wea. Forecasting* 7:410-429
- Koh TY, Ng JS (2009) Improved diagnostics for NWP verification in the tropics. *J. Geophys. Res.* 114:D12102, doi:10.1029/2008JD011179

Koh TY, Teo CK (2009) Towards a mesoscale observation network in Southeast Asia. *Bull. Amer. Meteor. Soc.* 90(4):481-488

Kolmogorov AN (1941) The local structure of turbulence in incompressible viscous fluid for very large Reynolds numbers. *C. R. Acad. Sci U.S.S.R.*, 30:pp301-305

Kolmogorov AN (1962) A refinement of previous hypotheses concerning the local structure of turbulence in a viscous incompressible fluid at high Reynolds number. *J. Fluid Mech.* 13:82-85

Kozu T, Reddy KK, Mori S, Thurai M, Ong JT, Rao DN, Shimomai T (2006) Seasonal and diurnal variations of raindrop size distribution in Asian monsoon region. *J. Meteor. Soc. Japan* 84A:195-209

Kumar P, Foufoula-Georgiou E (1993) A new look at rainfall fluctuations and scaling properties of spatial rainfall. *J. Appl. Meteorol.* 32:209-221

Lim JT, Samah AA (2004) *Weather and Climate of Malaysia*. Univ. Malaya Press, Kuala Lumpur, pp170

Lorenz EN (1963) Deterministic nonperiodic flow. *J. Atmos. Sci.* 20:130–141

Lovejoy S, Schertzer D (2008) Turbulence, raindrops and the $1\ 1/2$ number density law. *New J. of Physics* 10:075017-075032, doi:075010.071088/071367-072630/075010/075017/075017

Lovejoy S, Schertzer D, Allaire VC (2008) The remarkable wide range spatial scaling of TRMM precipitation. *Atmos. Res.* 90:10-32

Mandapaka PV, Lewandowski P, Eichinger WE, Krajewski WF (2009) Multiscaling analysis of high resolution space-time lidar-rainfall. *Nonlin. Processes Geophys.* 16:579-586

- Mandelbrot BB (1982) *The Fractal Geometry of Nature*. W. H. Freeman and Co., New York, pp468
- Marzban C, Sandgathe S (2009) Verification with variograms. *Wea. Forecasting* 24: 1102-1120
- Marzuki, Kozi T, Shimomai T, Hashiguchi H, Randeu WL, Vonnisa M (2010) Raindrop size distributions of convective rain over equatorial Indonesia during the first CPEA campaign. *Atmospheric Research* 96 (4): 645-655
- McBride JL, Ebert EE (2000) Verification of quantitative precipitation forecasts from operational numerical weather prediction models over Australia. *Wea. Forecasting* 15:103-121
- Menabde M, Harris D, Seed A, Austin G, Stow D (1997) Multiscaling properties of rainfall and bounded random cascades. *Water Resour. Res.* 33:2823-2830
- Mullen SL, Buizza R (2001) Quantitative precipitation forecasts over the United States by the ECMWF Ensemble Prediction System. *Mon. Wea. Rev.* 129:638–663
- Nikolopoulos EI, Kruger A, Krejewski WF, Williams CR, Gage KS (2008) Comparative rainfall data analysis from two vertically pointing radars, an optical disdrometer, and a rain gauge. *Nonlin. Processes Geophys.* 15: 987-997
- Nykanen D, Harris D (2003) Orographic influences on the multiscale statistical properties of precipitation. *J. Geophys. Res.* 108:8381, doi:10.1029/2001JD001518
- Obukhov A (1949) Structure of the temperature field in a turbulent flow, *Izv. Akad. Nauk SSSR*, 13: pp55–69
- Olsson J, Niemczynowicz J, Berndtsson R (1993) Fractal analysis of high-resolution rainfall time series. *J. Geophys. Res.* 98:23265–23274

Press WH, Teukolsky SA, Vetterling WT, Flannery BP (1992) Numerical Recipes in C: The art of scientific computing. 2nd ed Cambridge University Press

Schertzer D, Tchiguirinskaia I, Lovejoy S, Hubert P, Bendjoudi H, Larcheveque M (2002) Which chaos in the rainfall-runoff process? Hydrol. Sci. 47(1): 139-148

Sivakumar B, Liong SY, Liaw CY (1998) Evidence of chaotic behavior in Singapore rainfall. J. Am. Wat. Resour. Ass 34(2):301-310

Sivakumar B (2000) A preliminary investigation on the scaling behavior of rainfall observed in two different climates. Hydrol. Sci. 45(2):203-219

Tangang FT, Juneng L, Salimun E, Vinayachandran PN, Seng YK, Reason CJC, Behera SK, Yasunari T (2008) On the roles of the northeast cold surge, the Borneo vortex, the Madden-Julian Oscillation, and the Indian Ocean Dipole during the extreme 2006/2007 flood in southern Peninsular Malaysia. Geophys. Res. Lett. 35:L14S07, doi:10.1029/2008GL033429

Tessier Y, Lovejoy S, Schertzer D (1993) Universal multifractals: theory and observations for rain and clouds. J. Appl. Meteorol. 32:223-250

Tokay A, Kruger A, Krajewski WF, Kucera PA, Filho Pereira AJ (2002) Measurements of drop size distribution in the southwestern Amazon basin. J. Geophys. Res. 107:D20,doi:10.1029/2001JD000355

Torrence C, Compo GP (1998) A practical guide to wavelet analysis. Bull. Amer Meteorol. Soc. 79:61-78

Veneziano D, Bras RL, Niemann JD (1996) Nonlinearity and self-similarity of rainfall in time and a stochastic model. J. Geophys. Res. 101:26371-26392

Venugopal V, Foufoula-Georgiou E, Sapozhnikov V (1999) Evidence of dynamic scaling in space-time rainfall. *J. Geophys. Res.* 104:31599-31610

Verrier S, De Montera L, Barthès L, Mallet C (2010) Multifractal analysis of African monsoon rain fields, taking into account the zero rain-rate problem. *J. of Hydrol.* 389:111-120

White BG, Paegle J, Steenburgh WJ, Horel JD, Swanson RT, Cook LK, Onton DJ, Miles JG (1999) Short-term forecast validation of six models. *Wea. Forecasting* 14:84-108

Wilks DA (2006) *Statistical Methods in the Atmospheric Sciences*, 2nd ed., Academic, San Diego, Calif., pp627

List of Figures

Figure 1: The upper panel shows the model domain 1 and nested domains 2 to 5 with superimposed topographic height over Southeast Asia. The lower panel shows the domain 5 together with nested domain 6. The 8 rain gauge stations are: NTU, NUS, Tengah, Sembawang, MacRitchie, Sentosa, Paya Lebar and Changi, which are denoted by R1 to R8 respectively.

Figure 2: The spatial distributions of the rainfall at 2230 LT on 18 December 2006: [a] simulated rainfall in the nest 4 at the 0.9-km grid resolution, [b] observed radar reflectivity. The evaluation points 1 to 11 are shown in both panels.

Figure 3: [a, c, e] 10-minute, 5-minute and 1-minute time series of the simulated rainfall at the nearest grid point to R8, R2 and R1 stations respectively in the nest 4; [b, d, f] 10-minute, 5-minute and 1-minute record of observed rainfall at R8, R2 and R1 stations respectively. The thin horizontal line

denotes the precision limit of the rain gauges so that differences necessarily exist between the model and observation below this line.

Figure 4: The Fourier (solid grey lines) and wavelet (dotted blue lines) power spectra from 10-minute rainfall time series: panels [a], [c], [e] and [g] show the spectra from the observed rainfall from R1, R4, R6 and R8 stations, respectively; panels [b], [d], [f] and [h] show the corresponding spectra from the simulated rainfall in nest 4 at the model grid points nearest to these stations. Each solid red line is the least-square fit to the observed wavelet spectrum on the left panels from 60 (red dotted lines) to 20 minutes (shortest period in the spectra) and is duplicated onto the corresponding right panels. Their slopes are given on the lower left corner of the left panels. The black dashed lines denote the reference slope of $5/3$.

Figure 5: Assessment of observed spectral characteristics from 8 rain gauge stations: spectral slopes are bounded within one standard deviation from the least-squares fit to the observed wavelet spectra from 60 min to 20, 10 and 2 min for the 10-, 5- and 1-minute rainfall records, respectively. The solid and dashed horizontal lines represent the mean slope and its standard error bounds estimated from all stations in the 10- or 5-min datasets.

Figure 6: The Fourier (solid grey lines) and wavelet (dotted blue lines) power spectra from the simulated 10-minute rainfall for selected evaluation points (labelled on lower right corner) in the nest 4. The solid red lines in all panels are fixed with the best-estimate slope corresponding to $\beta_{10\text{min}} = 2.02$ from the 10-minute rain gauge data and have vertical intercepts that provide the least-square fit to the model wavelet spectrum between 60 and 20 min at each evaluation point. The black dashed line denotes the reference slope of $-5/3$.

Figure 7: Assessment of model spectral characteristics from the 11 evaluation points in nest 4: spectral slopes are bounded within one standard deviation from the least-squares fit to the model wavelet spectra from 60 min to 20 min. The solid and dashed horizontal lines represent the mean slope and its standard error bounds estimated from all 11 evaluation points. The data labelled “Obs” denote the best-estimate value from 10-min rainfall observation records for comparison.

Figure 8: The Fourier (solid grey lines) and wavelet (dotted blue lines) power spectra from 1-minute rainfall records: panel [a] shows the spectrum from the observed rainfall from R1 station; panels [b], [c] and [d] show the spectra from the simulated rainfall at the model grid point nearest to R1 station in the nests 4, 5 and 6, respectively. The solid red line in panel [a] is the least-square fit to the observed wavelet spectrum from 60 (red dotted line) to 2 minutes and is duplicated in the panels [b], [c] and [d]. The black dashed lines denote the reference slope of $-5/3$.

Figure 9: The Fourier (solid grey lines) and wavelet (dotted blue lines) power spectra from the simulated 1-minute rainfall at the model grid point nearest to R1 station in the nest 4 from the reduced time-step experiment. The black dashed lines denote the reference slope of $-5/3$.

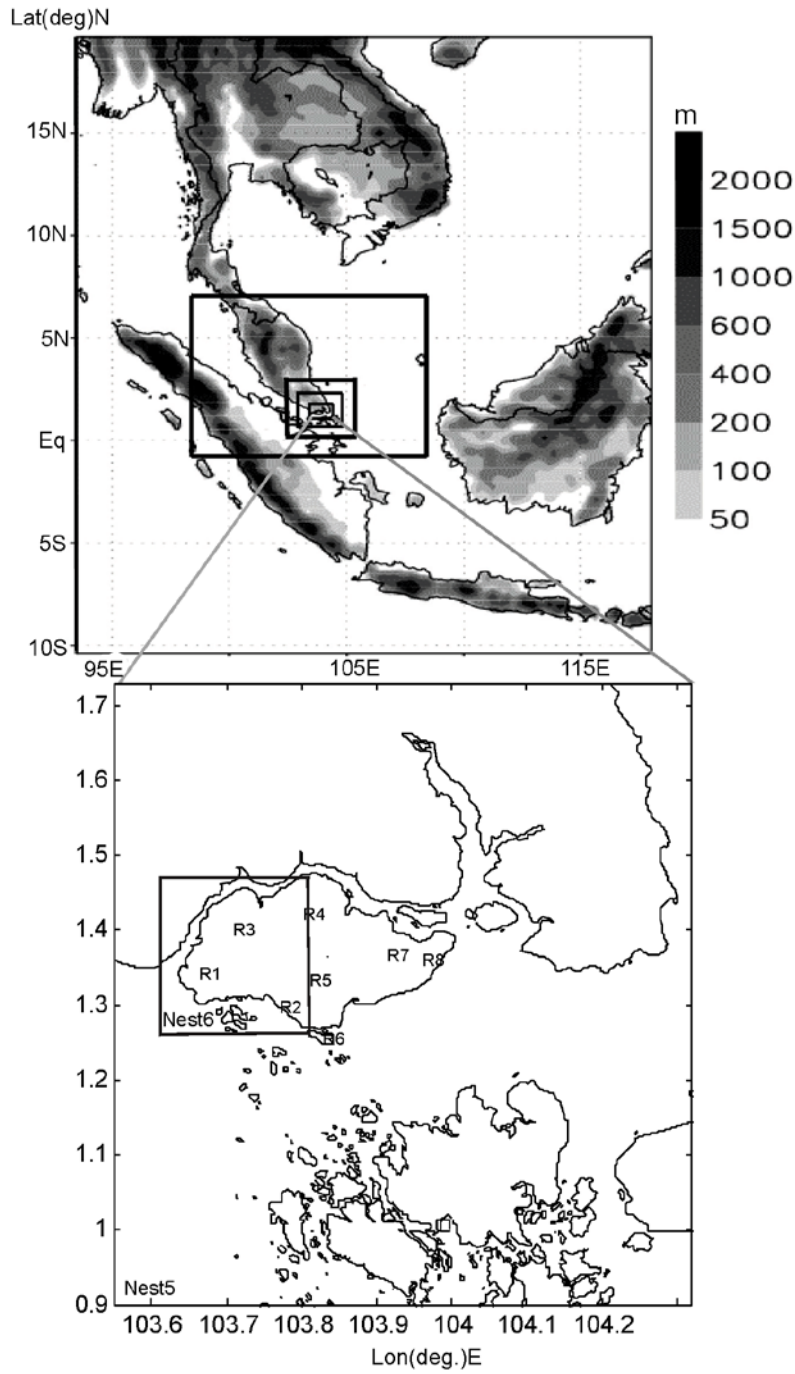


Figure 1: The upper panel shows the model domain 1 and nested domains 2 to 5 with superimposed topographic height over Southeast Asia. The lower panel shows the domain 5 together with nested domain 6. The 8 rain gauge stations are: NTU, NUS, Tengah, Sembawang, MacRitchie, Sentosa, Paya Lebar and Changi, which are denoted by R1 to R8 respectively.

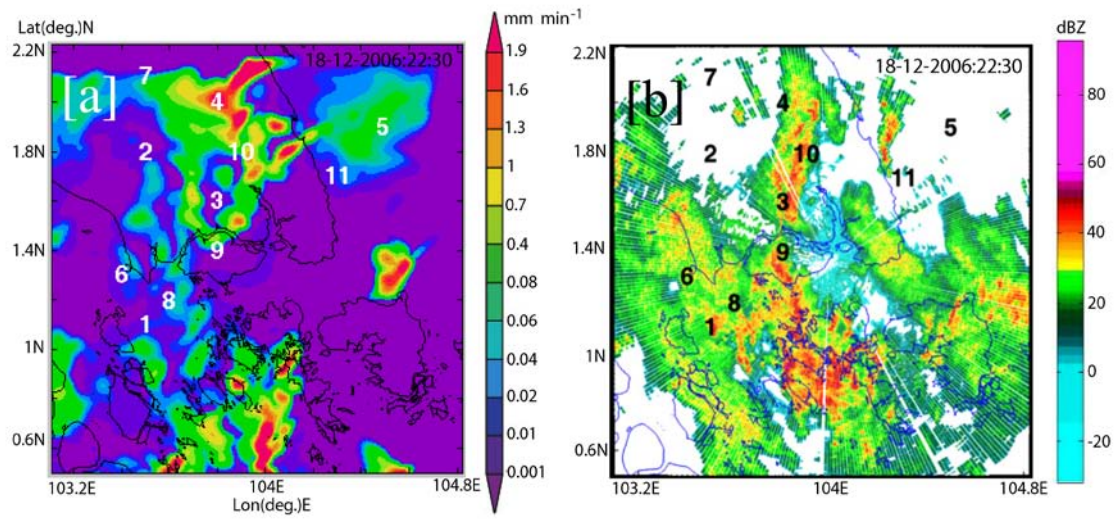


Figure 2: The spatial distributions of the rainfall at 2230 LT on 18 December 2006: [a] simulated rainfall in the nest 4 at the 0.9-km grid resolution, [b] observed radar reflectivity. The evaluation points 1 to 11 are shown in both panels.

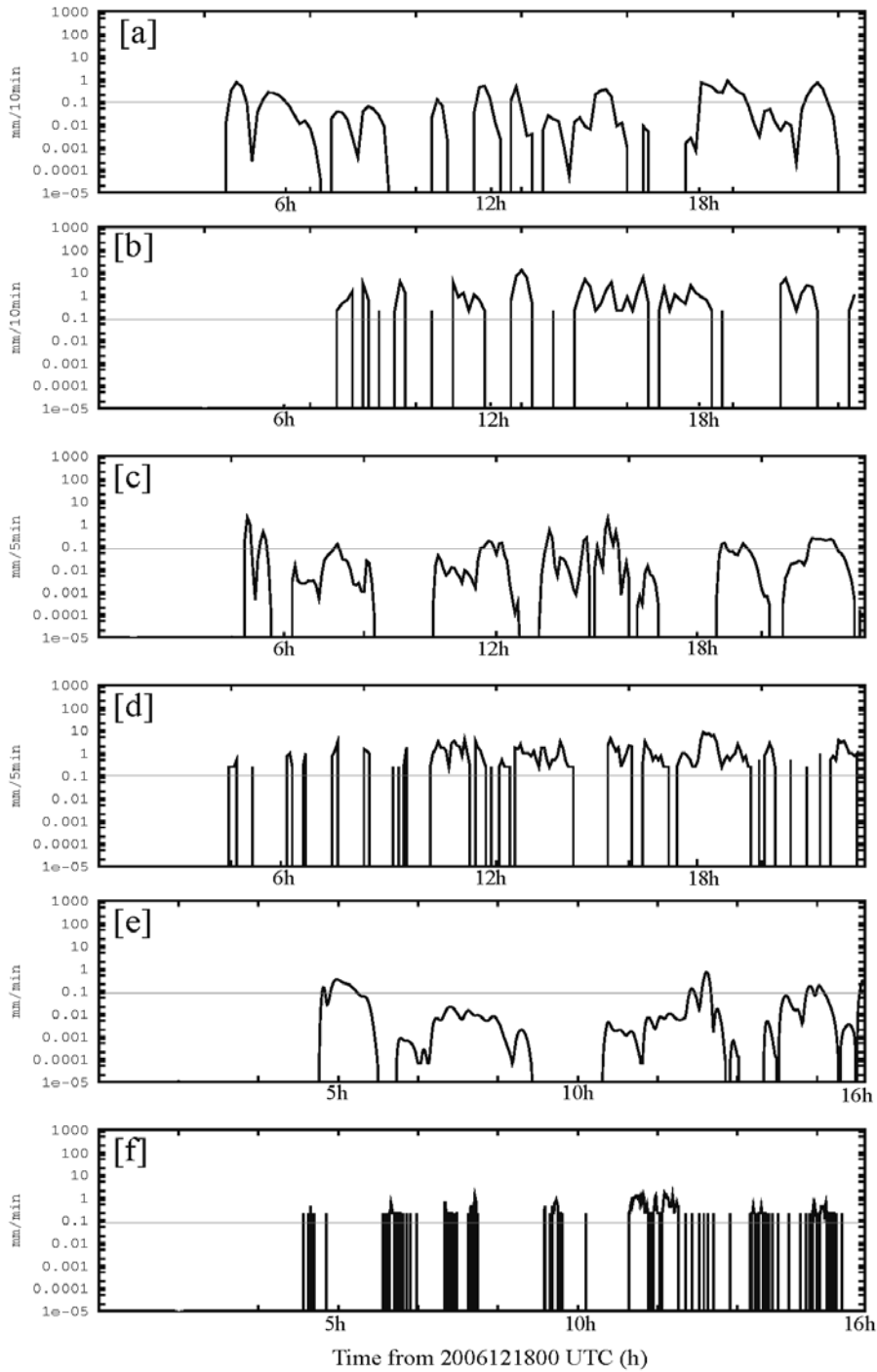


Figure 3: [a, c, e] 10-minute, 5-minute and 1-minute time series of the simulated rainfall at the nearest grid point to R8, R2 and R1 stations respectively in the nest 4; [b, d, f] 10-minute, 5-minute and 1-minute record of observed rainfall at R8, R2 and R1 stations respectively. The thin horizontal line denotes the precision limit of the rain gauges so that differences necessarily exist between the model and observation below this line.

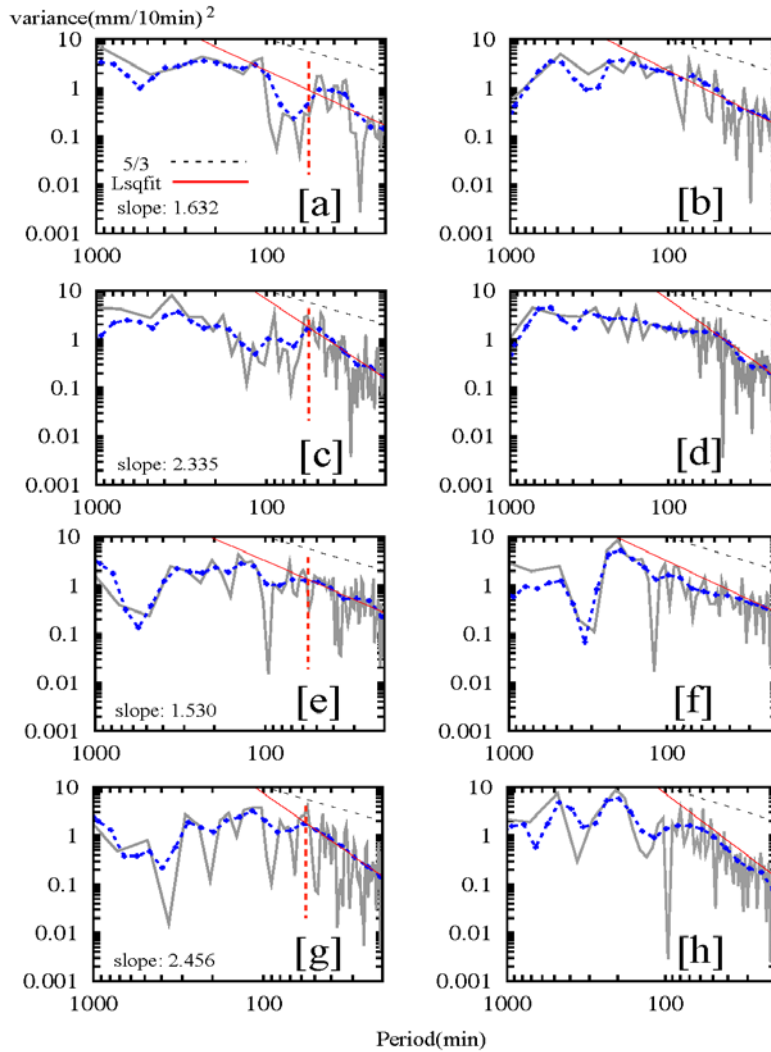


Figure 4: The Fourier (solid grey lines) and wavelet (dotted blue lines) power spectra from 10-minute rainfall time series: panels [a], [c], [e] and [g] show the spectra from the observed rainfall from R1, R4, R6 and R8 stations, respectively; panels [b], [d], [f] and [h] show the corresponding spectra from the simulated rainfall in nest 4 (0.9 km resolution) at the model grid points nearest to these stations. Each solid red line is the least-square fit to the observed wavelet spectrum on the left panels from 60 (red dotted lines) to 20 minutes (shortest period in the spectra) and is duplicated onto the corresponding right panels. Their slopes are given on the lower left corner of the left panels. The black dashed lines denote the reference slope of $5/3$.

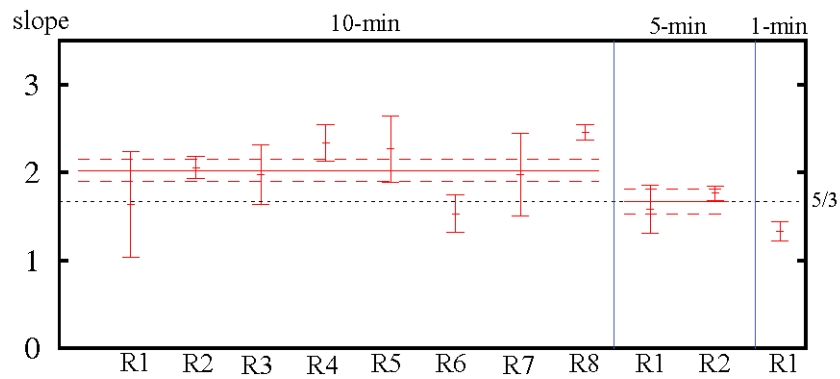


Figure 5: Assessment of observed spectral characteristics from 8 rain gauge stations: spectral slopes are bounded within one standard deviation from the least-squares fit to the observed wavelet spectra from 60 min to 20, 10 and 2 min for the 10-, 5- and 1-minute rainfall records, respectively. The solid and dashed horizontal lines represent the mean slope and its standard error bounds estimated from all stations in the 10- or 5-min datasets. The reference value of $\beta = 5/3$ is denoted by the dotted line.

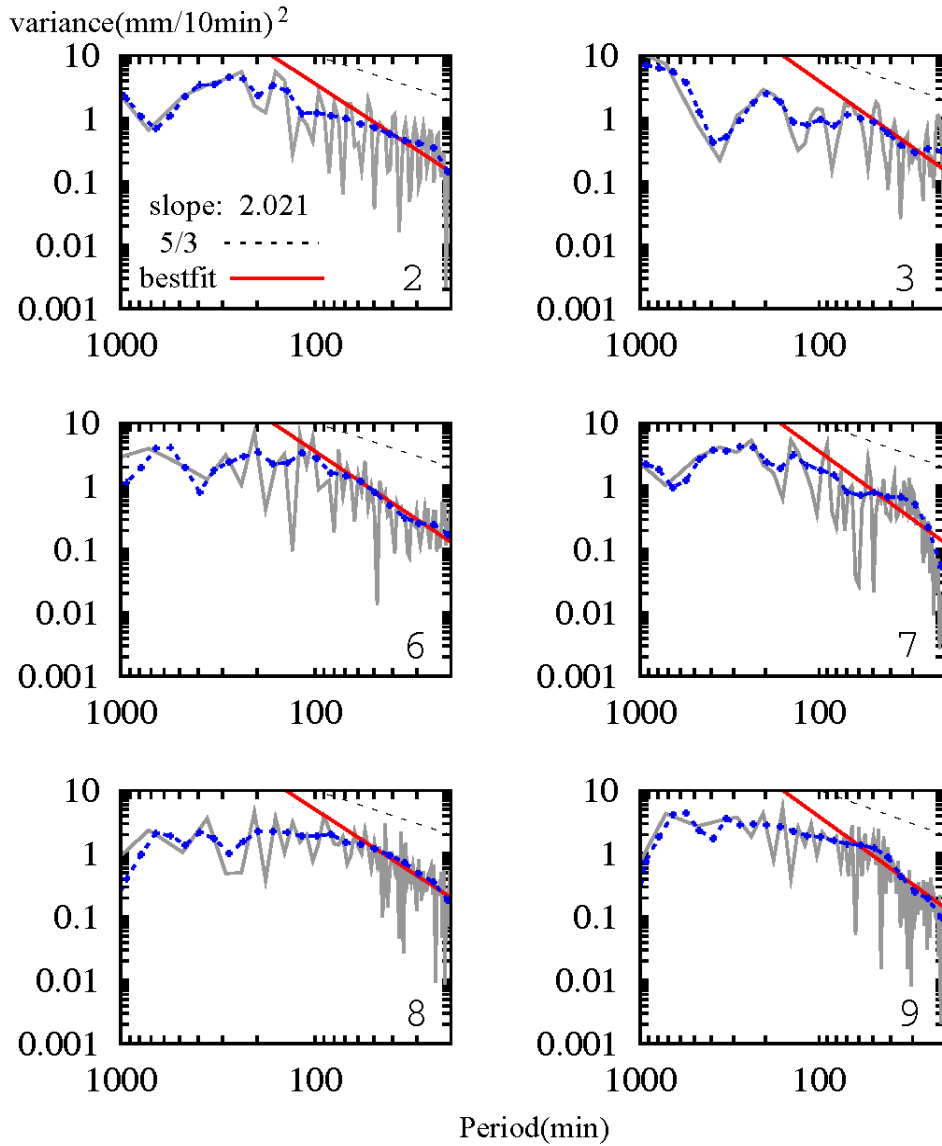


Figure 6: The Fourier (solid grey lines) and wavelet (dotted blue lines) power spectra from the simulated 10-minute rainfall for selected evaluation points (labelled on lower right corner) in the nest 4. The solid red lines in all panels are fixed with the best-estimate slope corresponding to $\beta_{10\text{min}} = 2.02$ from the 10-minute rain gauge data and have vertical intercepts that provide the least-square fit to the model wavelet spectrum between 60 and 20 min at each evaluation point. The black dashed line denotes the reference slope of 5/3.

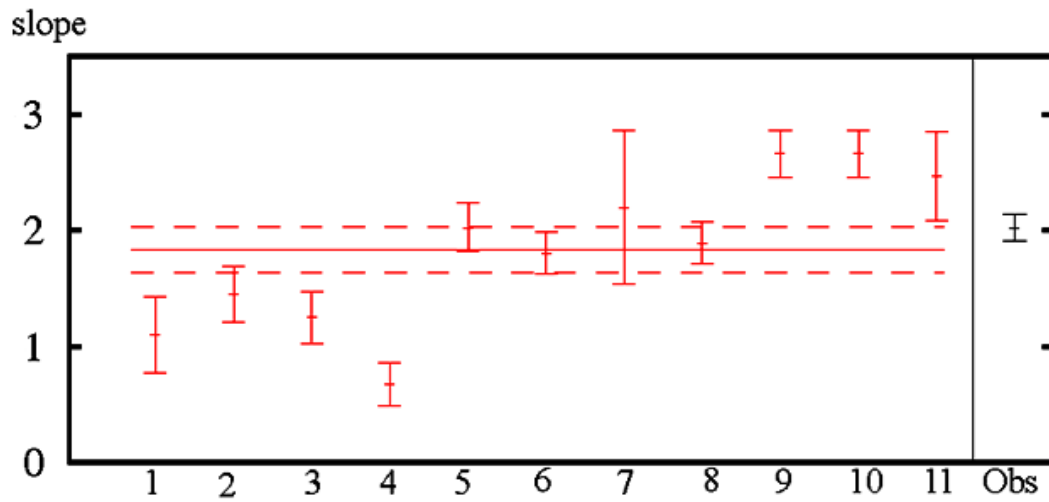


Figure 7: Assessment of model spectral characteristics from the 11 evaluation points in nest 4: spectral slopes are bounded within one standard deviation from the least-squares fit to the model wavelet spectra from 60 min to 20 min. The solid and dashed horizontal lines represent the mean slope and its standard error bounds estimated from all 11 evaluation points. The data labelled “Obs” denote the best-estimate value from 10-min rainfall observation records for comparison.

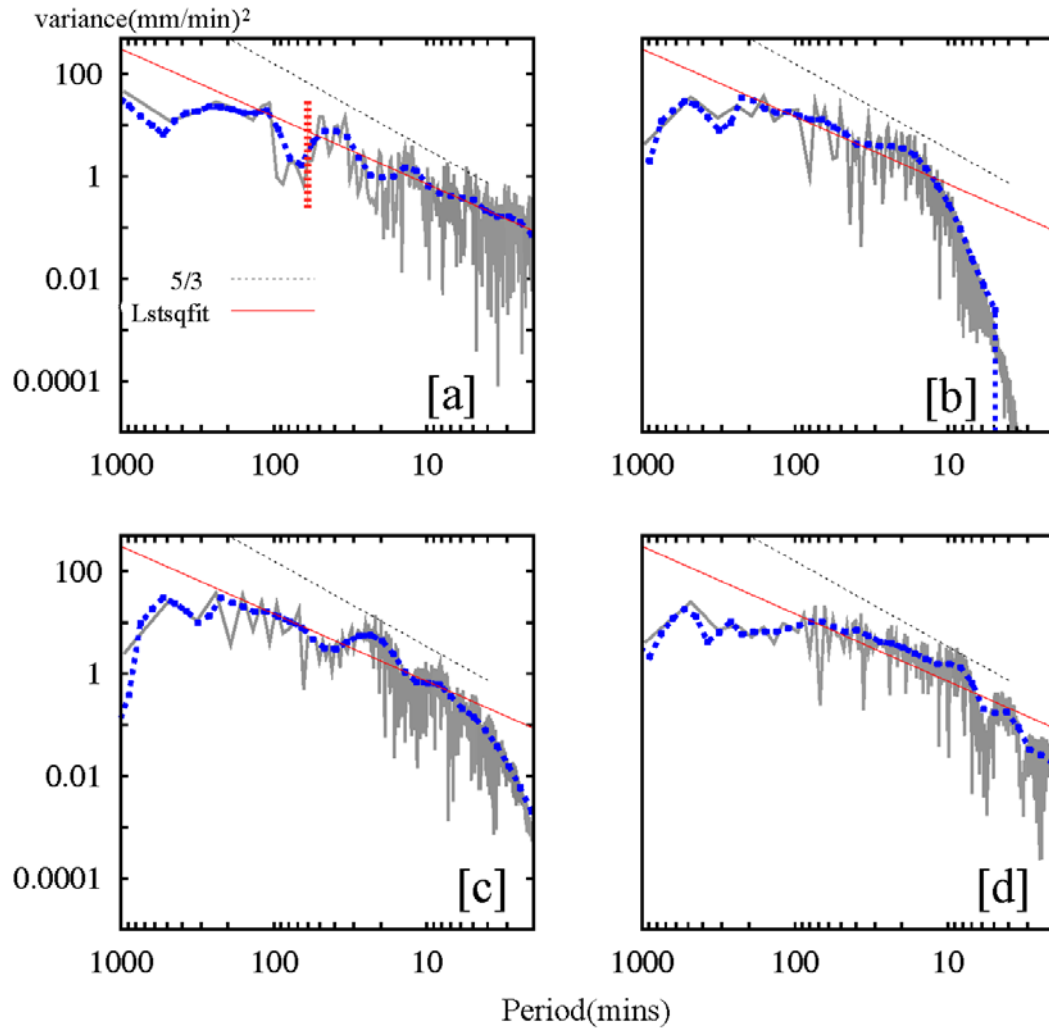


Figure 8: The Fourier (solid grey lines) and wavelet (dotted blue lines) power spectra from 1-minute rainfall records: panel [a] shows the spectrum from the observed rainfall from R1 station; panels [b], [c] and [d] show the spectra from the simulated rainfall at the model grid point nearest to R1 station in the nests 4, 5 and 6, respectively. The solid red line in panel [a] is the least-square fit to the observed wavelet spectrum from 60 (red dotted line) to 2 minutes and is duplicated in the panels [b], [c] and [d]. The black dashed lines denote the reference slope of $5/3$.

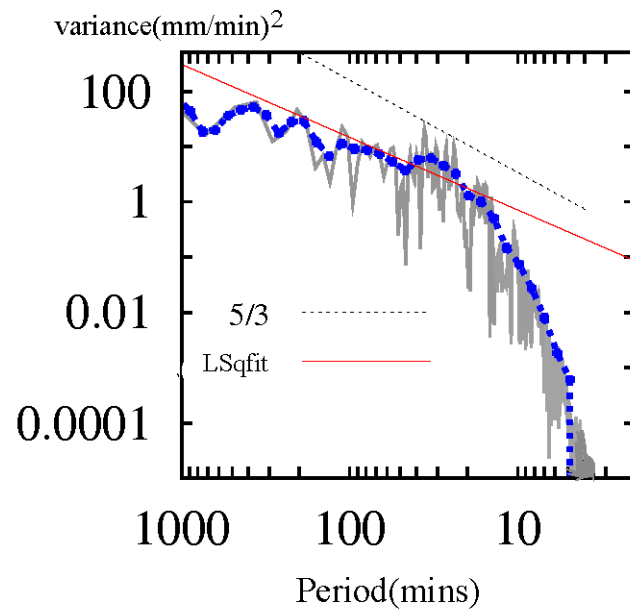


Figure 9: The Fourier (solid grey lines) and wavelet (dotted blue lines) power spectra from the simulated 1-minute rainfall at the model grid point nearest to R1 station in the nest 4 from the reduced time-step experiment. The black dashed lines denote the reference slope of $5/3$.